From the previous equations for m_r and σ_r of circular diaphragm we can be written these after added the pre-stress term in the following form:

$$\sigma_r = -z \left(\frac{E}{(1-v^2)} \left[\frac{\partial^2 w}{\partial r^2} + v \left(\frac{1}{r} \frac{\partial w}{\partial r} + \frac{1}{r^2} \frac{\partial^2 w}{\partial \theta^2} \right) + \alpha_T \frac{\Delta T}{h} (1-v) \right] + \frac{\sigma_0}{(1-v)} \right) \tag{13}$$

$$m_r = \int_{-(h/2)}^{+(h/2)} \sigma_r z dz = -D \left[\frac{\partial^2 w}{\partial r^2} + v \left(\frac{1}{r} \frac{\partial w}{\partial r} + \frac{1}{r^2} \frac{\partial^2 w}{\partial \theta^2} \right) + \alpha_T \frac{\Delta T}{h} (1-v) \right] + \frac{h^3 \sigma_0}{12(1-v)} \tag{14}$$

4. METHOD OF SOLUTION

When an applied loading and end restraints of the micro circular diaphragm are independent of the angle φ then the deflection of the diaphragm and the stress resultants and stress couples will depend upon the radial position r only. Such a bending of the circular diaphragm is referred to as axially symmetrical and the following simplifications can be made:

$$\frac{\partial^k ()}{\partial \theta^k} = m_{rt} = q_t = 0; \quad k = 1,2,3,4 \tag{15}$$

The differential equation of the deflected surface of the circular plate, Equation (10), reduces now to:

$$\frac{d^4 w}{dr^4} + \frac{2}{r} \frac{d^3 w}{dr^3} - \frac{1}{r^2} \frac{d^2 w}{dr^2} + \frac{1}{r^3} \frac{dw}{dr} = \frac{P + P_T}{D} \tag{16}$$

Eq. (16) appears in the form:

$$\frac{1}{r} \frac{d}{dr} \left\{ \frac{1}{r} \frac{d}{dr} \left[\frac{1}{r} \frac{d}{dr} \left(r \frac{dw}{dr} \right) \right] \right\} = \frac{P + P_T}{D} \tag{17}$$

Where Eq. (17) the governing partial differential equation of the axisymmetric thermo-mechanical bending of circular diaphragm and w is the deflection of the diaphragm at axial direction we can be obtained by solve the partial differential Eq. (17).

Rigorous solution of Eq. (17) is obtained as the sum of the complementary solution of the homogeneous differential equation, w_h, and the particular solution, w_p, i.e.,

$$w = w_h + w_p \tag{18}$$

The complementary solution of Equation (17) is given by:

$$w_h = C_1 \ln r + C_2 r^2 \ln r + C_3 r^2 + C_4 \tag{19}$$

Where C_i $(i = 1,2,3,4)$ are constants that can be evaluated from the boundary conditions. The particular solution, w_p, is obtained by successive integration of Eq. (17):

$$w_p = \int \frac{1}{r} \int r \int \frac{1}{r} \int \frac{r(P(r) + P_T(r))}{D} dr dr dr dr \tag{20}$$

4.1 The boundary conditions

The boundary conditions for micro circular diaphragm with clamped edge as shown in Fig.2 are:

$$
\left. \begin{array}{l} w = 0|_{r=a} \\ \frac{\partial w}{\partial r} = 0\Big|_{a=0} \end{array} \right\}
\tag{21}
$$

For the solid plate, which contains no concentrated loads at $r=0$, it is easy to see that the terms involving the logarithms in Eq. (19) yield an infinite displacement and bending moment, and the shear force for all values of C_1 and C_2, except zero; therefore, $C_1 = C_2 = 0$. Thus, for a solid circular plate subjected to an axisymmetric distributed load with arbitrary boundary conditions, the deflection surface is given by:

$$
w = C_3 r^2 + C_4 + w_p
\tag{22}
$$

The constants of integration C_3 and C_4 in this equation are determined from boundary conditions and we obtain:

$$
C_3 = -\frac{Pa^2}{32D} - \frac{m_T}{D}\left[\frac{1}{4}\ln a - \frac{1}{8}\right]
\tag{23}
$$

$$
C_4 = \frac{Pa^4}{64D} + \frac{a^2 m_T}{8D}
\tag{24}
$$

And after some manipulation, the transverse deflection w, bending moments (m_r, m_t) and shear forces (q_r) will becomes:

$$
w = \frac{P}{64D}(a^2 - r^2)^2 + \frac{m_T}{4D}r^2(\ln r - \ln a) + \frac{m_T}{8D}(a^2 - 3r^2)
\tag{25}
$$

$$
m_r = \frac{P}{16}\left(a^2(v+1) - r^2(3+v)\right) + \frac{m_T}{2}(v+1)(\ln a - \ln r) - \frac{m_T}{2} - D\alpha_T\frac{\Delta T}{h}(1-v) + \frac{h^3\sigma_0}{12(1-v)}
\tag{26}
$$

$$
m_t = \frac{P}{16}\left(a^2(v+1) - r^2(1+3v)\right) + \frac{m_T}{2}(v+1)(\ln a - \ln r) - \frac{m_T}{2}v - D\alpha_T\frac{\Delta T}{h}(1-v)
\tag{27}
$$

$$
q_r = -\frac{Pr}{2}
\tag{28}
$$

5. RESULTS AND DISCUSSION

In this section, some analytical numerical results are presented for micro circular diaphragm has the geometrical properties of 2a = 1 mm and about 0.1 mm thickness (see section (2)). The diaphragm is first pre-stress under radial stress σ_0 then clamped between two plates. The diaphragm is made of one of common material which used in numerous micro electro-mechanical sensors (memes) and bioengineering applications;

this material is pure aluminum which mechanical and thermal properties are given in Table 1. Table 2 show the mechanical and thermal Loading history applied on the micro Circular Diaphragm .

Table 1 Material thermal and mechanical properties

Material	E (Gpa)	G (Gpa)	υ	K (W.C^{-1}. m^{-1})	α (C^{-1})
Al-Pure	71.7	26.9	0.333	237	23 E-6

Table 2 Loading history

Pressure P (MPa)	P_1 = 100	P_2 = 200	P_3 = 300	P_4 = 400
Temperature T_b (C$^{\circ}$)	T_1 = 50	T_2 = 100	T_3 = 150	T_4 = 200

5.1 Analytical Results

The mechanical behavior of micro circular diaphragm under the previous conditions that have been mentioned we can be discussed in Figs. 4-5. Figs. 4 (a)-(f) shows the relation between transverse deflection w, bending moments (m_r, m_t), shear force (q_r) and stress (S_r, S_t) respectively with the micro circular diaphragm radius (r) under varying pressure (P). As shown in the Fig. 4(a) the transverse deflection w is decreased with diaphragm radius (r) and increased with pressure (P) and the maximum deflection occurs at the center of the plate at $r=0$. Figs. 4(b)-(c) show the bending moment diagram of radial and tangential moment where increased with pressure (P) and the residual moment due to pre-stress is appear in the Fig. 4(b) and the maximum bending moment (m_r, m_t) are occurs at ($r = a$, $r = 0$) respectively. As shown in Fig. 4(d) the shear force (q_r) is increased with both diaphragm radius and pressure, and the maximum shear force occurs at the at the edge of the plate at $r = a$. Figs. 4(e)-(f) show the stress at radial and tangential direction of diaphragm where increased with pressure (P) and the pre-stress is appear in Fig. 4(e).
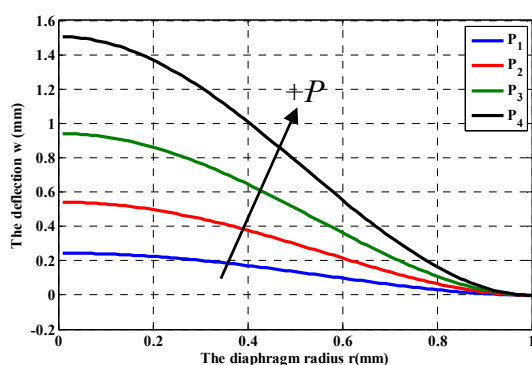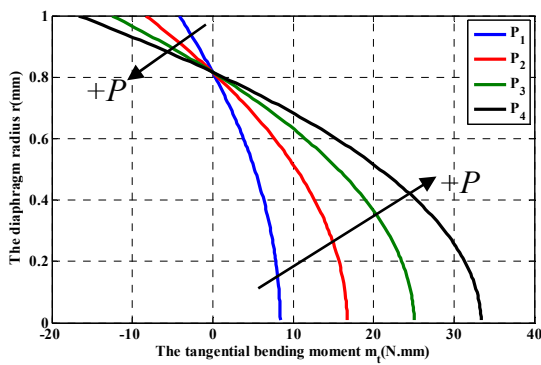

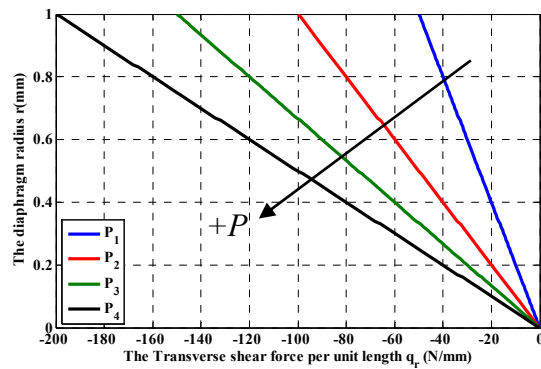(a) Transverse deflection w
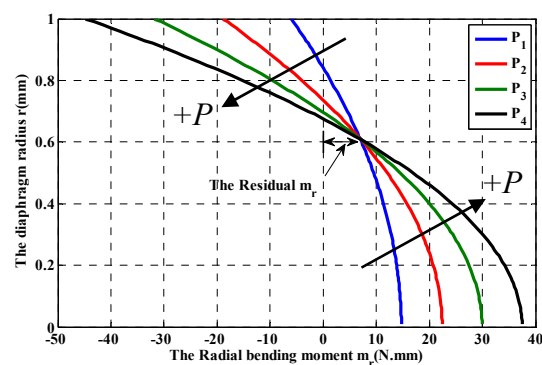
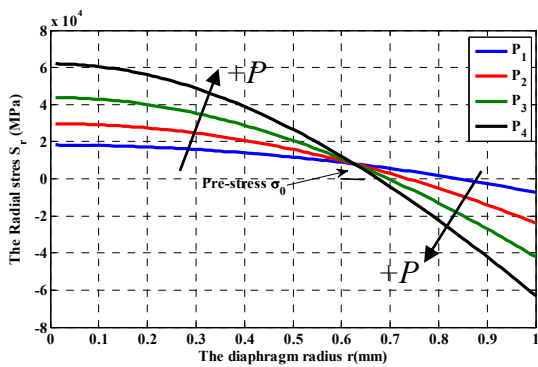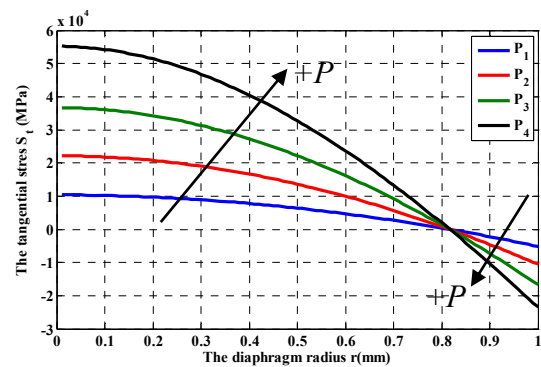(b) Radial bending moment m_r

(c) Tangential bending moment m_t

(d) Shear force q_r

(e) Radial stress S_r

(f) Tangential stress S_t

Fig. 4 The relation between the micro circular diaphragm radius (*r*) and the mechanical characteristics under varying applying pressure (*P*) for all target material.

Fig. 5 shows the relation between the radial stress S_r and radial strain e_r , where the radial strain e_r is increased with radial stress S_r. This relation is very important in engineering analysis where the Young's modulus *E* of the diaphragm material from the slop of this liner relation.
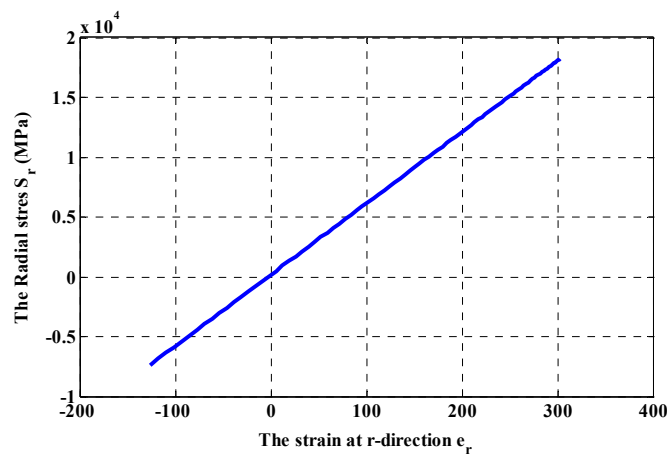

Fig. 5 The relation between the radial stress S_r and radial strain e_r

The thermal behavior of micro circular diaphragm under the previous conditions that have been mentioned we can be discussed in Fig. 6. Fig. 6(a)-(b) show the relation between bending moments (m_r, m_t) respectively with the micro circular diaphragm radius (*r*) under varying temperature (T_b), where the maximum bending moments are increased with temperature (T_b).
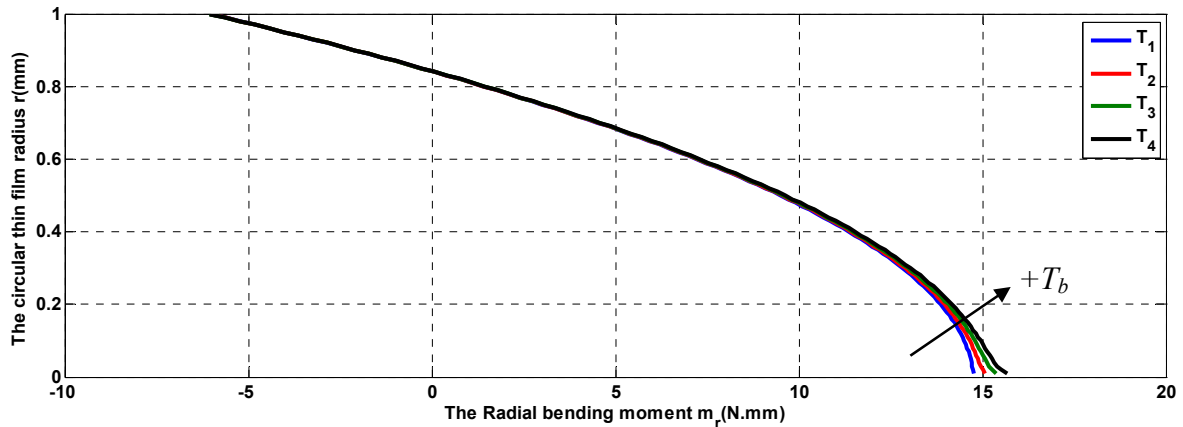

(a) Radial bending moment m_r
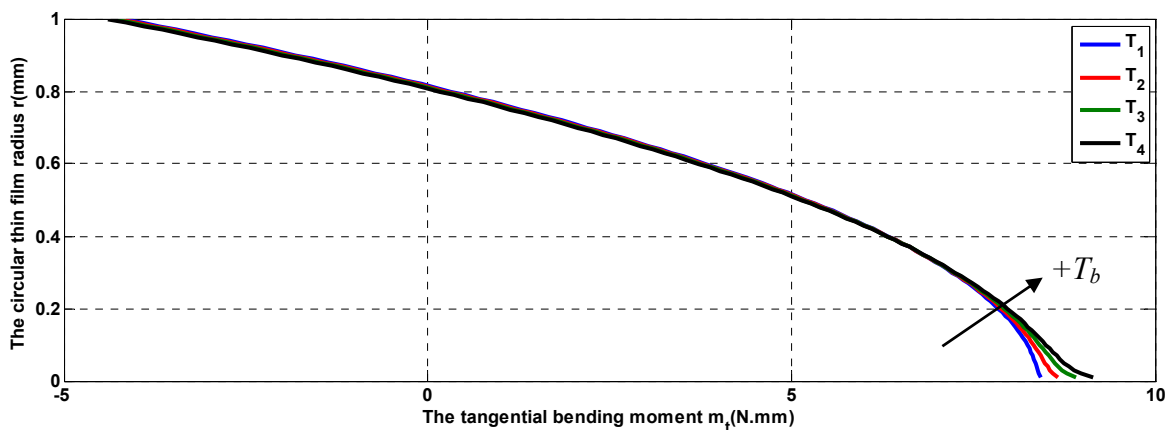


(b) Tangential bending moment m_t

Fig. 6 The relation between the micro circular diaphragm radius (*r*) and the mechanical characteristics under varying temperature (T_b).
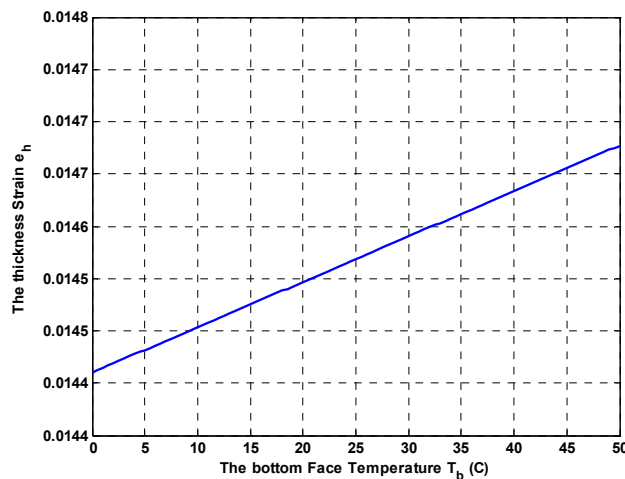
<u>Thickness Deformation</u>   Fig. 7 shows the micro circular diaphragm thickness deformation behavior across the diaphragm radius (*r*) under varying pressure (*P*) and temperature (*T_b*). As shown in the Fig.5 (a) the dome thickness (*h*) is increased with diaphragm radius *r* and decreased with pressure (*P*), the thickness strain e_h in the Fig. 7 (b)-(c) is increased with the pressure (*P*) and temperature (*T_b*) respectively.
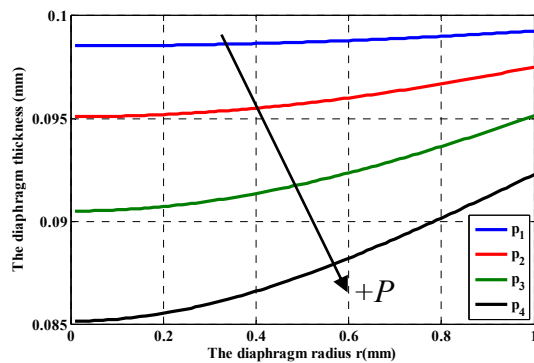
(a) The relation between dome thickness *h* and the diaphragm radius r under varying pressure *P*
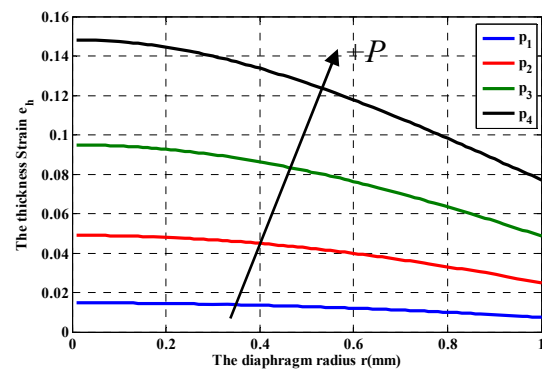
(b) The relation between the thickness strain e_h and the diaphragm radius r under varying pressure *P*

(c) The relation between the thickness strain e_h and the diaphragm bottom face temperature T_b

Fig. 7 The micro circular diaphragm thickness deformation behavior across the diaphragm radius (*r*) under varying pressure (*P*) and temperature (T_b)

5.2 Numerical Results

The finite element simulation for the bulge test of micro circular diaphragm under the previous conditions that have been mentioned we can be discussed in Fig. 8. Fig. 8 shows the deformation history of micro circular diaphragm in both 3D Mesh mode and contour mode at applied pressure $P= P_1 = 100$ *MPa*. As shown in the Fig. 8 the maximum deflection occurs at the center of the plate at *r=0*, the maximum deflection w_{max} is found 0.24 mm. If we compared the maximum deflection from a finite element simulation model and another one from analytical calculus we are found that they are closed.

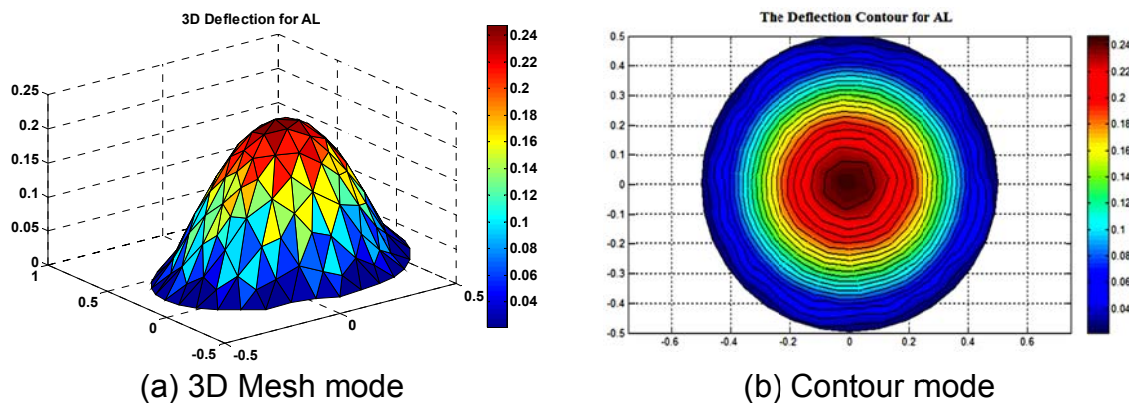(a) 3D Mesh mode   (b) Contour mode

Fig. 8 The finite element simulation for the bulge test of micro circular diaphragm
by using MATLAB PDE tool box

6. CONCLUSION

In this paper, both analytical and numerical analysis of bulge test technique for micro circular diaphragm subjected to thermal and mechanical load has been shown. In the analytical analysis we have derived the partial differential equation of the micro circular diaphragm. The mechanical and thermal curves of the material flow is plotted and discussed. The thickness distribution across the diaphragm radius is discussed to describe the mechanical behavior of the micro circular diaphragm under deformation. The finite element simulation for the bulge test of micro circular diaphragm has been shown for the same conditions of the analytical calculus and the comparison between them has been to accuracy and validity of proposed technique. It was found from the results of the comparison the convergence is occurred between the finite element model and analytical model.

REFERENCES

Saute W., (2000), 'Thin Film Mechanics –Bulging And Stretching'. PhD thesis, Mechanical Engineering, University of Vermont.

Hill R., (1950), 'A theory of plastic bulging of a metal diaphragm by lateral pressure', Phil. Mag. (ser 7) 41.

Mellor P.B., (1956), Stretch forming under fluid pressure, J. Mech. Phys. Solids 5.

Swift H. W., (1952), 'Plastic instability under plane stress', J. Mechanics and Physics of Solids, Vol. 1, pp. 1 to 18.

Chater E. and Neale K. W., (1983), 'Finite plastic deformation of a circular membrane under hydrostatic pressure-I', J. Mech. Sci. Vol. 25, No. 4, pp. 219-233.

Storakers B., (1966), 'Finite plastic deformation of a circular membrane under hydrostatic pressure', J. Mech. Sci. Vol. 8, pp. 619-628.

Zeghloul A., Mesrar R. and Ferron G., (1991), 'Influence of material parameters on the hydrostatic bulging of a circular diaphragm', J. Mech. Scl. Vol. 33, No. 3, pp. 229-243.

Wang N. M. and Shammamy M. R., (1969), O'n the plastic bulging of a circular diaphragm by hydrostatic pressure', J.M ech.Ph ys. Solid1s, Vo1.7,pp 43-64.

Ilahi M. F., Parmar A. and Mellor P. B., (1981), 'Hydrostatic bulging of a circular aluminum diaphragm', Int. J. Mech. Sci. Vol. 23, pp. 221-227.

Itozaki H., (1982), 'Mechanical properties of composition modulated copper-palladium foils', Ph.D. Dissertation, Northwestern University, Evanston, IL.

Small M.K. and Nix W.D., (1992), 'Analysis of the accuracy of the bulge test in determining the mechanical properties of thin-films', J. Mater. Res. 7, 1553.

Vlassak J.J., (1994), 'New experimental techniques and analysis methods for the study of mechanical properties of materials in small volumes', Ph.D. Dissertation, Stanford University, Stanford, CA.

Xiang Y., Chen X., Vlassak J.J., (2005), 'Plane-strain bulge test for thin films', J. Materials Research Society, 20, pp.2360-2370.